Advances in Water Resources 32 (2009) 1011–1019

Contents lists available at ScienceDirect

Advances in Water Resources

journal homepage: www.elsevier.com/locate/advwatres

Rainfall spatial variability observed by X-band weather radar and its implication for the accuracy of rainfall estimates

E. Moreau *, J. Testud, E. Le Bouar

NOVIMET, 10-12 Avenue de l'Europe, 78140 Velizy, France

ARTICLE INFO

Article history:
Received 7 February 2008
Received in revised form 17 November 2008
Accepted 18 November 2008
Available online 3 December 2008

Keywords:
Quantitative precipitation estimation (QPE)
X-band radar

ABSTRACT

The main objective of this paper is to estimate the error in the rainfall derived from a polarimetric X-band radar, by comparison with the corresponding estimate of a rain gauge network. However the present analysis also considers the errors inherent to rain gauge, in particular instrumental and representativeness errors. A special emphasis is addressed to the spatial variability of the rainfall in order to appreciate the representativeness error of the rain gauge with respect to the 1 km square average, typical of the radar derived estimate. For this purpose the spatial correlation function of the rainfall is analyzed.

The data set consists of 1-year radar data collected by the X-band polarimetric radar HYDRIX®, located in Beauce region (80 km south of Paris). All data were processed in real time using the ZPHI® algorithm. A dense 25 rain gauge network provided ground comparison data.

The various sources of uncertainties (instrumental and representativeness) are then analyzed and quantified for each sensor.

1. Introduction

Improving all kind of water management will be a major issue in the near future. Population growth, improvement of the standard of living, agricultural practices, and the extension of irrigated surfaces increase the pressure on the water resource, particularly limited in semi-arid regions. Meanwhile, for many climate scientists, the global warming will be a problem not so much by the direct effect of temperature increase but through the induced change in the rainfall regime [10]. For this purpose, it would help greatly to have available accurate information concerning rainfall. Rain is recognized as a highly intermittent phenomenon, extremely variable in geographic space. According to a recent study, Gebremichael and Krajewski [6] (denoted hereafter by GK), the correlation radius for tropical rain, derived from a dense gauge network, is about 4 km with a time integration of 15 min. Nowadays two types of measurement devices are available and operational: rain gauges and weather radar. The rain gauge is a reliable instrument having the full confidence of hydrologists but it is a point measurement. The weather radar is able to provide a continuous and long range description of the rain field. It helps to monitor the evolution of weather systems and thus allows the anticipation of the weather at a given location. But the accuracy of its estimate is subject to caution [8].

The main objective of this paper is to estimate the error in the rainfall derived by a polarimetric X-band radar as compared to rain gauges. A special emphasis is addressed to the spatial variability of the rainfall in order to estimate the representativeness error of the rain gauge with respect to the 1 km square pixel of the radar analysis. The spatial rain variability is characterized by the spatial correlation function estimated from the data. This paper uses the GK method for computing the spatial correlation function derived from point (gauge) or area (radar) data.

This question of rain gauge representativeness error related to the small-scale variability of the rain was addressed in previous papers. Ciach and Krajewski [2] proposed a method for estimating the radar rainfall error variance, assuming that the radar gauge differences can be partitioned into the error of the radar estimate and the gauge representativeness error. This approach named "error variance separation" (EVS) was recently revisited by Zhang et al. [16] and the influence of sub-grid scale information was found to be crucial. This paper follows a similar approach with the aim to separate the instrumental and representativeness errors attached to each sensor.

Our purpose in the present study is to evaluate the capability of an X-band polarimetric radar to measure rainfall (despite the attenuation by rain at this frequency band). The first part is dedicated to the algorithm ZPHI® [14,1] used to extract the rainfall from the polarimetric radar measurements. Two other algorithms are also used for comparison purposes, based on a classical Z–R relation ship, with and without correction of the reflectivity for attenuation All radar derived rain products are evaluated by

* Corresponding author.
E-mail addresses: emmanuel.moreau@novimet.com (E. Moreau), jacques.testud@novimet.com (J. Testud), erwan.lebouar@novimet.com (E. Le Bouar).

0309-1708/$ - see front matter © 2008 Elsevier Ltd. All rights reserved.
doi:10.1016/j.advwatres.2008.11.007

comparison with gauge measurements. The second part is focused on the characterization of the rain spatial variability. Spatial correlation function derived from the gauge network and from the various rains radar products are then compared, according to the approach proposed by GK. Then, a new method is proposed to derive the instrumental and the representativeness error of both instruments.

2. Experimental setup

The radar data used in this study comes from an X band dual polarization radar (named HYDRIX®). This "compact" radar (antenna diameter is 1.2 m) uses the hybrid technology (i.e. simultaneous transmission of H&V polarizations). More technical information about this radar can be found in Table 1.

The HYDRIX® radar was deployed on October 2004, on the roof of a building of Arvalis-Institut-du-Végétal, an agricultural institute located 70 km south of Paris, France. A very simple scanning strategy was applied: a scanning back and forth in a limited azimuth sector of 75° (between 200° and 275° East of North) at a single elevation (1.8°) and at the speed of 3 deg/s. The validation network (24 rain gauges and one disdrometer) was deployed in the azimuth sector covered by the radar and within 25 km range from the radar (illustrated in Fig. 1). The purpose of this strategy was

1. To limit drastically the sampling error of the radar thanks to an exceptionally short revisit time (60 s at most and 30 s on average).
2. To limit the radar representativeness error since the altitude of the center of the beam is between 160 m at 5 km range and 850 m at 25 km range.
3. To limit the radar error due to non uniform beam filling, since the beam width ranges from 175 m at 5 km from the radar to 875 m at 25 km.

During the reference period October 2004 to October 2005, the radar produced 14,745 estimates of the 6-min rainfall over the 24 rain gauges of the network, representing a total rainfall of 307 mm (average at each rain gauge site).

The HYDRIX radar data was processed in real time with the ZPHI® algorithm [14]. ZPHI® operates in three steps: first, it corrects the observed reflectivity for along path attenuation; second it derives the N_0^* parameter of the drop size distribution [15]; third, it retrieves the rain rate using the universal Z–R relationship parameterized by N_0^* given by

$$R = a(N_0^*)^{1-b}Z^b \tag{1}$$

with a = 9.306E-5, b = 0.603. Thus, the N_0^* adjustment takes account of the natural variability of the drop size distribution known to be a major cause of uncertainty in the Z–R relationship.

The radar rain rates were then interpolated in a 1 km^2 resolution geographic grid, using Cressman filtering [4]. They were also time integrated primarily over 6 min to fit the rain gauge time sampling.

Table 1
Main specifications of HYDRIX prototype.

Frequency	9.4 GHz
Peak transmit power	16 kW per channel
Antenna	1.2 m
Antenna gain	38.5 dB
Scan velocity	3 deg/s in azimuth
Beam width	2 deg
Pulse length	0.5–2 μs
Pulse repetition frequency	500 Hz
Sensitivity	0 dBZ at 12.5 km or 25 km
Polarization mode	Simultaneous H and V

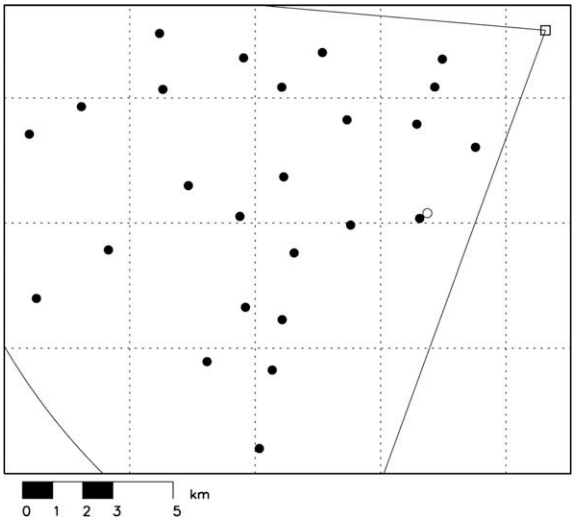

Fig. 1. layout of the rain gauge network (●), the radar (□) and the disdrometer (○). The sector covered by the radar is display (limited to 25 km range).

The two other algorithms considered for comparison, are based on a "classical" Z–R relationship, in fact the Z–R relation (1) in which N_0^* is set to the constant value ($10^{6.4}$ m^{-4}), corresponding to the mean N_0^* measured by the disdrometer during the field campaign. One algorithm uses the original reflectivity Z (attenuated by rain) and the other the reflectivity Z_c corrected for attenuation by ZPHI®.

In the following the three rainfall rate estimates are referred to as "standard ZPHI®", "classical Z–R", and "attenuation corrected Z_c–R".

3. Radar algorithm comparison

All rain products have been accumulated over 1hr. Fig. 2 summarizes the point-by-point comparison of the hourly rainfall measured by the rain gauges and by the radar during the reference period. The corresponding statistical characteristics are given in Table 2 in terms of Pearson correlation coefficient:

$$r = \frac{\sum_{i=1}^{n} x_i y_i - n\bar{x}\bar{y}}{(n-1)s_x s_y} \tag{2a}$$

and Nash criterion [11]:

$$\text{Nash} = 1 - \frac{\sum_{i=1}^{n}(x_i - y_i)^2}{\sum_{i=1}^{n}(y_i - \bar{y})^2} \tag{2b}$$

where $\bar{x}$ and $\bar{y}$ are the sample means, s_x and s_y the sample standard deviation.

The scatter plot with the classical Z–R estimator is negatively biased, especially for higher rainfall, due to attenuation. The scatter plot for the "attenuation corrected Z_c–R" estimate has a slight positive bias, but is almost as spread as the "classical Z–R" estimate. The standard ZPHI® estimate is slightly negatively biased, and its scatter is reduced with respect to the previous estimates. The Pearson correlation coefficient and the Nash criterion are substantially improved not only with respect to the "classical Z–R", but also with respect to the "attenuation corrected Z_c–R". The performance of ZPHI® is due to two factors: first, the relationship between specific attenuation and rain rate is naturally less scattered than the Z–R relationship, and second, the ray-by-ray adjustment of N_0^* allows the effect of the natural variability of the DSD to be considerably reduced.

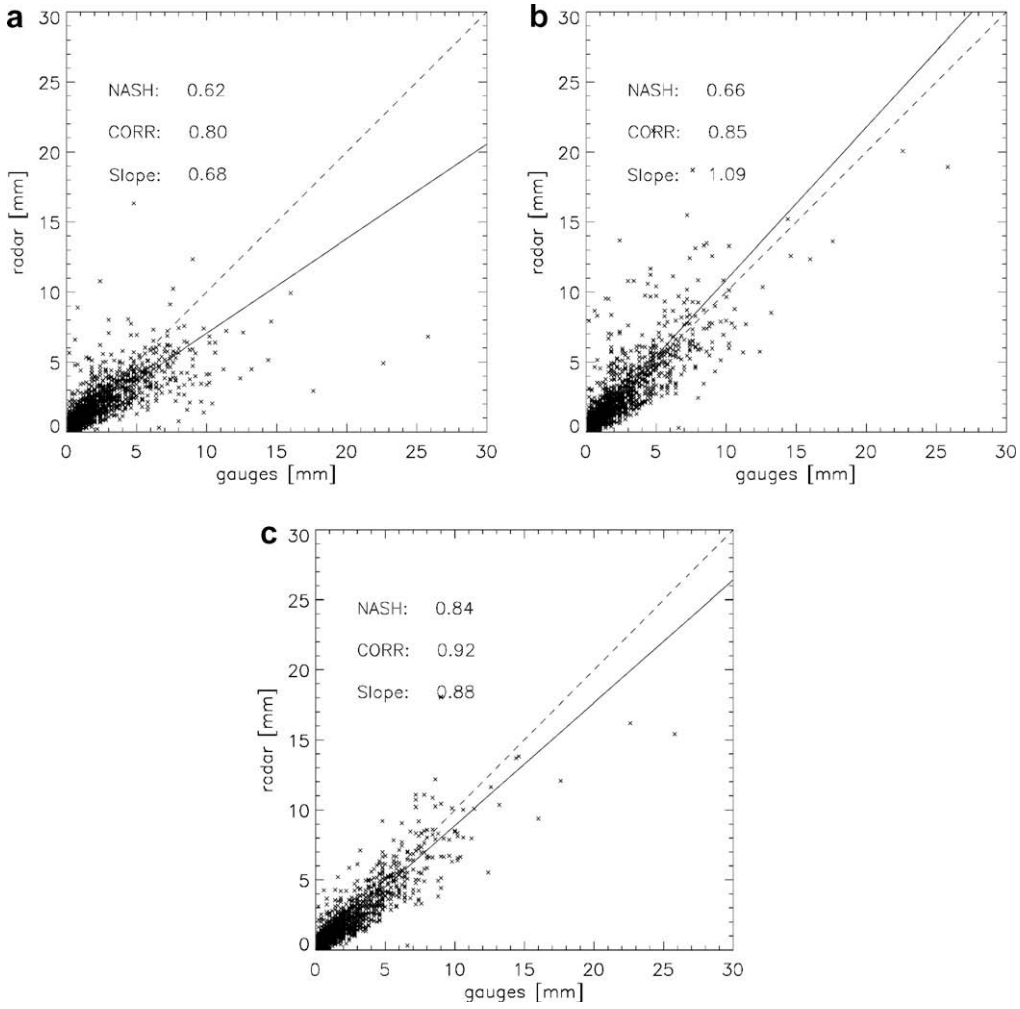

Fig. 2. Point by point comparison of hourly rainfall observed by the radar (vertical axis) and the rain gauges (horizontal axis) – 13 months of data October 2004–2005. The radar estimate is interpolated at the rain gauge site. (a) "Classical Z–R" estimate. Upper (b) "attenuation corrected Z_c–R" estimate. (c) Standard "ZPHI® estimate".

Table 2
Statistical characteristics of the comparison between the radar estimates and the rain gauges (slope of the regression line, Pearson correlation coefficient, Nash criterion, mean, variance and relative bias). One hour accumulation is considered.

	Slope	Pearson	Nash criterion	Mean (mm)	Variance (mm^2)
Rain gauges	nc	nc	nc	1.279	3.380
Classical Z–R	0.68	0.80	0.62	1.147	1.805
Attenuation corrected Z_c–R	1.09	0.85	0.66	1.361	3.875
Standard ZPHI®	0.88	0.92	0.84	1.25	2.664

This comparison clearly shows the benefits of the ZPHI® algorithm compared to the two others. Nevertheless, at this point, the gauges are considered as the "true" reference and part of the errors found in the comparisons comes from the gauges. Two types of errors have to be considered, the instrumental error and the representativeness error. The latter can be estimated by the knowledge of the small-scale rain variability.

4. Rain variability observed by radar and gauges

A spatial correlation analysis has been carried out to characterize the rain variability. This analysis is based on the procedure described by GK and originally developed by Shimizu [13].

Fig. 3 displays the spatial correlation function for the 6 min rainfall, estimated from the 24 rain gauge network, together with the correlation function calculated for two radar estimates: standard ZPHI® and "classical Z–R". The whole data set (1 year period) is considered. For the radar estimates, the sampling is restricted to the same locations as the rain gauge sites. For the theoretical representation of the correlation function, we consider the three-parameter exponential model (GK):

$$\rho(h) = \rho_0 \exp(-(h/R_0)^F) \tag{3a}$$

where h is the separation distance, F is the shape parameter, R_0 is the correlation radius (km), and ρ_0 defines the nugget parameter. The nugget parameter is the local decorrelation that can be caused by microscale variability or by random instrumental errors. A standard least square fit routine is used to adjust the shape parameter F and the correlation radius R_0 for determining the best fit to the experimental points. The minimum distance between the gauges in the network was not small enough (>1.2 km) to accurately determine the nugget parameter. Based on very dense rain gauge network, Krajewski et al. [9] found that for time scale of 15min or larger, ρ_0 attains a level of about 0.95–0.97 depending on the climate regime. For the fit, the nugget parameter is fixed to 0.97 by default for all cases. When analyzing the radar data, the fitting curve is no longer given as in (3a), representing the point correlation function, but the area (1×1 km^2) correlation function $\rho_A(h)$:

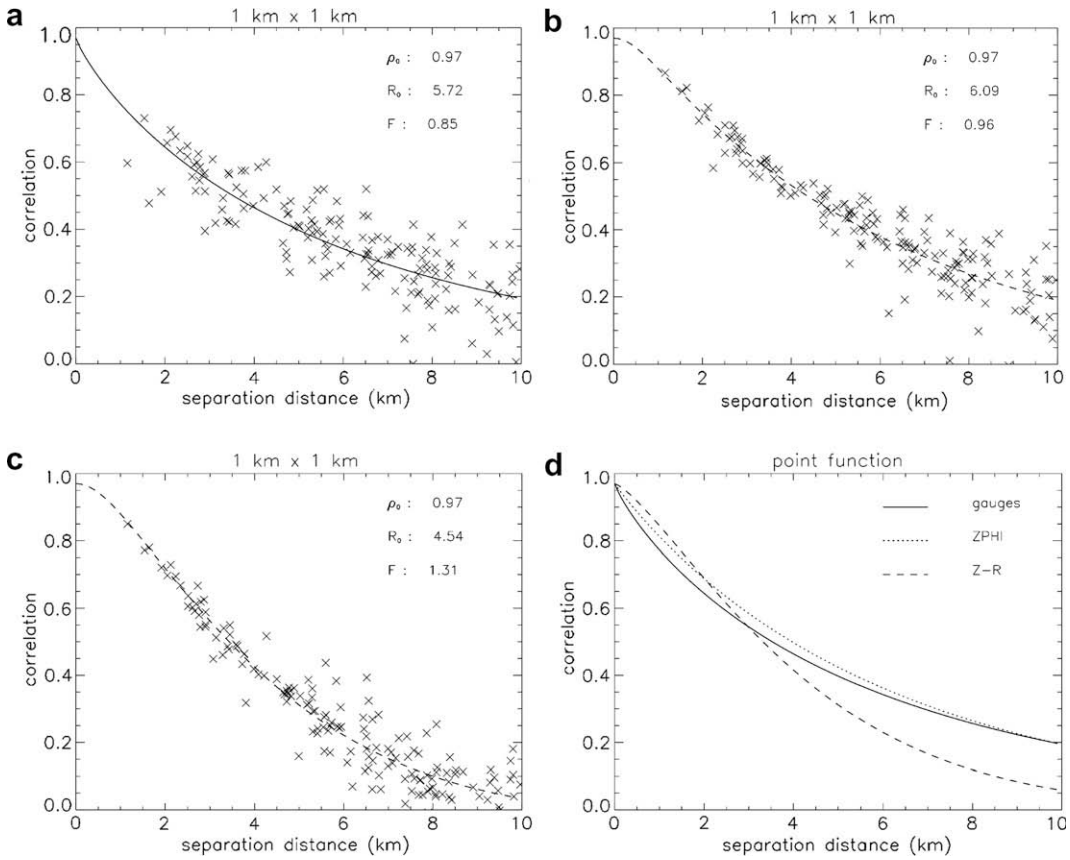

Fig. 3. Spatial correlation function of the 6 min rainfall, derived from the 24-rain gauge network (a); from the ZPHI® radar estimate (b); from the classical radar estimate (c). For the radar estimates, the sampling is restricted to the same locations as the rain gauge sites. The continuous line in (a) is the model adjustment for point measurement (relevant for the rain gauge network). The broken line in (b) and (c) is the model adjustment for 1×1 km^2 area measurements (relevant for the radar). (d) Compares the "point correlation functions" derived from the three data sources.

$$\rho_A(h) = \mathrm{cov}_A[h]/\mathrm{var}[R_A(x,y)] \tag{3b}$$

where $\mathrm{var}[R_A(x, y)]$ and $\mathrm{cov}_A[h]$ are the variance and covariance function for the random field $R_A(x,y)$, as defined in Eqs. (5a) and (6) of GK, respectively. These area variance and covariance are related to the point correlation function $\rho(h)$ through the functional $\gamma(L, L)$ defined by

$$\gamma(L,L) = \left(\frac{2}{L}\right)^2 \int_0^L dh_x \int_0^L dh_y \left(1 - \frac{h_x}{L}\right)\left(1 - \frac{h_y}{L}\right)\rho(h) \tag{3c}$$

where h_x and h_y are the separation distances in x and y, $h = \sqrt{(h_x^2 + h_y^2)}$ and L the side-length of the square area A.

From their analysis of TRMM-LBA and TEFLUN-B data, GK observed that the correlation function determined from the radar dropped faster (meaning a shorter correlation radius) than the one determined from the rain gauge network. They argued from their results that the radar derived rainfall product should be less accurate than the rain gauge one. A similar observation can be made in this paper when comparing correlation function derived from the "classical Z–R" and from the rain gauge (Fig. 3a and c). However, the correlation function for ZPHI® rainfall estimates turns out to be very close to the one for the rain gauge network (Fig. 3b and d). Using the same argument as GK, one tends to deduce that the "classical Z–R" estimate is less accurate than the rain gauges, while the "standard ZPHI®" estimate is of similar accuracy as the rain gauges.

The reason of improved comparison of correlation functions in this paper [when using ZPHI® estimate] with respect to GK deserves some comments:

(1) The scanning strategy in this experiment is more favorable: 30 s revisit time instead of 5 or 10 min in GK, reducing the time sampling error.
(2) The distance of the rain gauge network to the radar site is closer: 15 km on average, instead of 40–50 km in GK, reducing the radar representativeness error.
(3) The type of event, probably less convective in the Boigneville experiment than in TRMM-LBA and TEFLUN-B. It is to be noted that the correlation radius of the 6 mn rainfall is about 6 km in this experiment and about 4 km in GK.
(4) The improved performance of ZPHI®. This improvement would not be due to the correction for attenuation (since S band radars are used in GK), but to the N_0^* adjustment.

In the framework of the experiment at Boigneville (France), estimating the spatial correlation function from the rain gauge required about one year of data, in order to obtain enough samples. In opposite, the larger area covered by the radar, with a spatial resolution of 1 km^2, allows the spatial correlation to be accurately estimated from a few rain events only. In the following, one month of rain radar data (October 2004) over the area covered by the gauge network is selected to estimate the rain spatial variability. Figs. 4 and 5 display the spatial correlation derived from the radar data, for 6 min and 1 h rain accumulations, respectively. The spatial area correlation is fitted by ρ_A Eq. (3b) using a Gradient-expansion nonlinear least square algorithm. The three-parameter exponential point correlation ρ is related to the ρ_A function through Eq. (3c) and therefore is estimated during the minimization process. We can notice the almost perfect fit of the area corre-

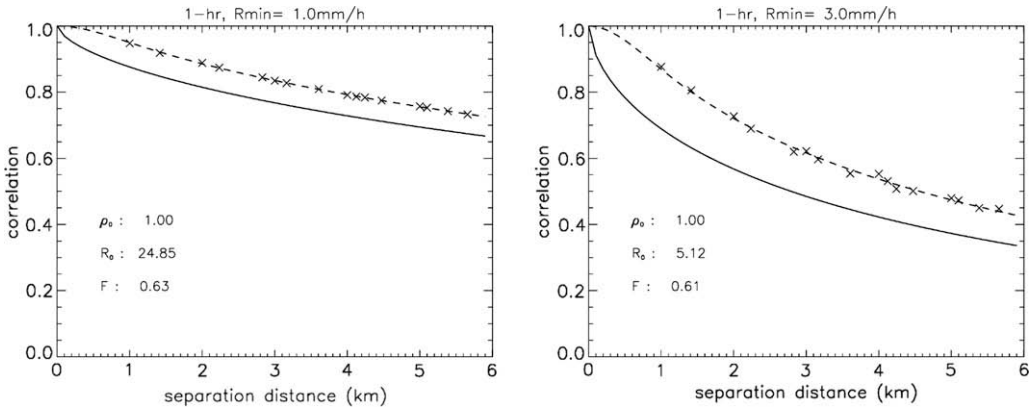

Fig. 4. Spatial correlation derived from one month (October 2004) of hourly rain retrieved from radar measurements by ZPHI® over the whole scan. The fitted function $\rho_A(h)$ and the associated $\rho(h)$ are represented by the dash and the solid line, respectively. At the top (resp. bottom), only rain rates larger than 1 mm/h (resp. 3 mm/h) are considered.

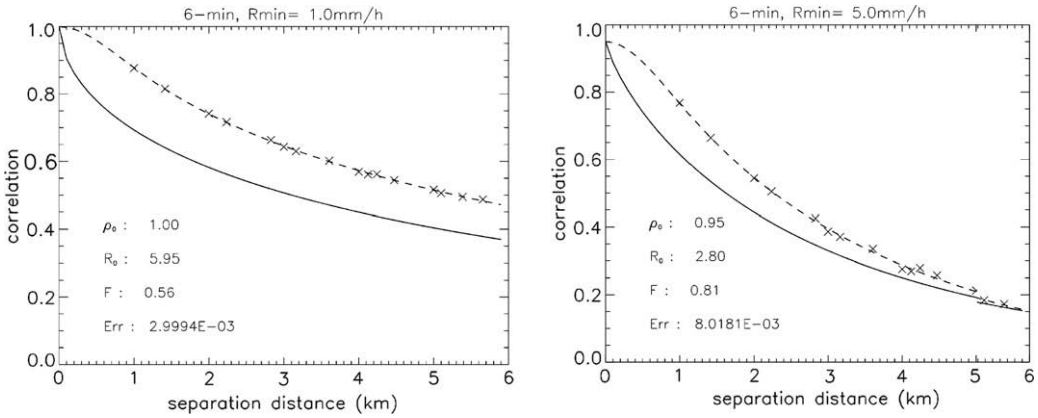

Fig. 5. Spatial correlation derived from one month (October 2004) of 6 mn rain retrieved from radar measurements by ZPHI®. The fitted function $\rho_A(h)$ and the associated $\rho(h)$ are represented by the dash and the solid line, respectively. At the top (resp. bottom), only rain rates larger than 1 mm/h (resp. 5 mm/h) are considered.

lation function ρ_A over the radar data. The scatter about the fit is negligible, compared to Fig. 3b. This can be explained by the more extended sampling available to compute the correlation (by a factor of ten). The nugget parameter is very close to 1.0 because only due to random instrumental errors of the radar. The microscale scale representation error is here filtered by the analysis at 1 km^2 pixel.

The spatial point correlation function $\rho(h)$ (i.e. the one that would be obtained from rain gauge measurements), also plotted in Figs. 4 and 5, exhibits lower correlations up to 8 km separation distance, for all cases. A large reduction is observed at short distances and for the more convective events ($F < 1$). The correlation radius decreases rapidly when considering only higher rainfall rates. For 1hr rain rates, R_0 drops to 5 km when selecting rain rates higher than 3 mm/h. The same tendency can be observed for the 6 min rain rates. Habib and Krajewski [7] observed a correlation radius of 2 km for 15 min heavy rain accumulation with a dense rain network, during the TEFLUN-B field campaign in Florida.

5. Instrumental and representativeness errors

As mentioned before, comparison of gauge and radar estimates is problematic because of the difference in sampling strategy of the two instruments. The catchment area of the rain gauge is very small (~0.1 m^2), but its sampling is continuous in time. The radar diffusive volume at a particular range gate has a ground projection of the order of the reference pixel of 1 km^2 presently considered, but the radar sampling in time consists of snapshots whose spacing is the revisit time. Considering the spatial and temporal rain variability (for temporal variability, see for example Paulson [12]), we expect significant representation errors for both instruments.

Considering first the radar error, the "instrumental error" may be derived from Eq. (1) as

$$\frac{\delta R}{R} = \frac{1}{b}\frac{\delta Z}{Z} - \frac{(1-b)}{b}\delta \ln(N_0^*) \tag{4}$$

The first term $T1$ on the right hand side of Eq. (4) is proportional to the relative error in Z. For signal to noise ratio greater than 10 (this is always the case with rainfall measurement), according to the radar measurement theory, $\delta Z/Z$ is proportional to $N_i^{-0.5}$ (where N_i is the number of independent samples [5]) itself proportional to $M^{-0.5}$ (where M is the number of samples, only defined by the radar pulse repetition frequency and scanning velocity). M is a fairly constant parameter, given the radar operating mode. The coefficient of proportionality slightly depends on the velocity variance (variable with the type of event – convective or stratiform – not with the rain rate).

Considering the second term $T2$ on the right hand side of Eq. (4), if a classical algorithm is used (which implies that N_0^* is set to a fixed value), $T2$ expresses a relative error in R due to the natural spread of N_0^*. There is no evidence that this spread is related to the amplitude of R. The ZPHI® estimate is less concerned by $T2$ since ZPHI® resolves N_0^*. Thus, it can be said that the radar instrumental error is by essence a multiplicative error. Moreover, there is

no strong argument to consider a dependence of this multiplicative error with the R amplitude.

The local random error related to tipping–bucket rain gauge measurements can originate from several sources such as bucket sampling effect, hydrodynamic water flow instabilities in the gauge funnels and differences in the wind effect caused by turbulent airflow around the rain gauges [3]. The first two sources are directly related to the instrument itself as the last effect is related to microscale turbulence in the atmosphere. Ciach [3] found, based on a cluster of 15 rain gauge deployed over an area of 8 m × 8 m, that the standard deviation of the relative errors can be expressed by an monotonically decreasing function: $\sigma_m = E_0(T) + R_0(T)/R_T$, where E_0 and R_0 are function of the accumulation time T (for 1-h rain accumulation $\sigma_m = 0.004 + 0.2/R_T \sim 0.2/R_T$). Therefore, the standard deviation of the absolute error can be approximated by a constant value (~0.2 mm/h for 1-h rain accumulation).

We define the instrumental error A_{rad} attached to the radar, by

$$R_{\text{rad}} = A_{\text{rad}} R \tag{5a}$$

and for the gauge error B_g related to bucket sampling, by

$$R_g = r + B_g \tag{5b}$$

where R_{rad} denotes the radar rainfall estimates over the area A (1 km^2) and R_g the gauge rainfall at a certain point within the area, r stands for the true point rainfall, R the true area-averaged rainfall defined by $R = \int_A r\,dx$.

In (5a) the error A_{rad} is assumed multiplicative, independent of the rainfall intensity, lognormally distributed. Some justification was above given about the multiplicative character of the radar derived rain estimate. The hypothesis that A_{rad} is in addition independent of R means that the relative error is constant (hence the absolute error grows proportionally to R). We are conscious that this hypothesis of independence is imperfect and mainly dictated by convenience to perform the calculation. But it is probably the best we can do with our present knowledge.

Similarly, in (5b), it is assumed that the error B_g, additive and normally distributed, is independent of the rainfall intensity. B_g represents the resolution of the tipping bucket (0.2 mm). It is a absolute error.

All previously defined errors are assumed not biased; this will be discussed further later:

$$E(A_{\text{rad}}) = 1 \quad \text{and} \quad E(B_g) = 0 \tag{6}$$

The standard error for the radar is defined as follows:

$$\varepsilon_{\text{rad-inst}} = \sqrt{\text{var}(A_{\text{rad}})}$$

As the error in the rain gauge estimate is absolute, in order to be able to compare it with the radar estimate, a normalization is practiced as

$$\varepsilon_{g\text{-inst}} = \sqrt{\frac{\text{var}(B_g)}{E(r^2)}} \tag{7}$$

with $\text{var}(B_g) = (0.2\ \text{mm/h})^2$.$\varepsilon_{g\text{-inst}}$ is referred to in the following as the "relative error" in the rain gauge estimate.

However, it should be noticed that the normalization by $E(r^2)$ is somewhat arbitrary. A different normalization could produce somewhat different results.

Similarly, the normalized representativeness error is defined by

$$\varepsilon_{\text{rep}} = \sqrt{\frac{\text{var}(r-R)}{E(R^2)}} \tag{8}$$

where $E(\,)$ and var( ) are the expectation and variance operators, respectively.

The point-area difference variance divided by the point variance can be expressed, as in Ciach and Krajewski [2], by

$$\begin{aligned}\frac{\text{var}(r-R)}{\text{var}(r)} &= 1 - \frac{2}{A}\rho_0 \int_A \tilde{\rho}(x, x_g)\,dx^2 + \frac{1}{A^2}\rho_0 \int_A \\ &\quad \times \int_A \tilde{\rho}(x,y)\,dx^2\,dy^2 \\ &= 1 - 2f_3 + f_1\end{aligned} \tag{9a}$$

and

$$\begin{aligned}\text{var}(R) &= \text{var}(r) f_1 \\ \text{cov}(r,R) &= \text{var}(r) f_3\end{aligned} \tag{9b}$$

where x_g denotes the location of the gauge within the area and cov() is the covariance operator. The point correlation function $\tilde{\rho} = \rho/\rho_0$ denotes the spatial correlation assuming no local decorrelation. The nugget parameter ρ_0 reflects the microscale variability in the rain fields and the random measurement errors of the rain gauges. As mentioned before, the rain gauge network used in this study is not dense enough to accurately estimate this parameter from the spatial correlation. Therefore, the nugget parameter is left as a free parameter that would be estimated, as explained in the following. We notice in Eq. (9a) the needs of the relative position of the gauge in the area. Because all gauges are not located at the same position with respect to the radar pixels, a spatial interpolation is performed on the radar data at the gauge location. Therefore, each location of the gauge is at the center of the area and the first integral function in Eq. (9a) remains the same for all gauges.

The variance of the difference between the rain radar and the rain gauge can be expressed as

$$\text{var}(R_g - R_{\text{rad}}) = \text{var}(R_g) + \text{var}(R_{\text{rad}}) - 2\text{cov}(R_g, R_{\text{rad}}) \tag{10}$$

The last term in Eq. (10), the covariance between the rain radar and the rain gauge, can be written as

$$\text{cov}(R_g, R_{\text{rad}}) = E(R_g, R_{\text{rad}}) - E(R_g)E(R_{\text{rad}}) \tag{11}$$

Substituting R_g and R_{rad} by Eq. (5a) and (5b) in (11) and considering that errors are not biased and independent of the rainfall, leads to

$$\text{cov}(R_g, R_{\text{rad}}) = E(rR) - E(r)E(R) = \text{cov}(r,R) \tag{12}$$

The covariance between the point and the area-average rainfall can be estimated by substituting Eqs. (10) into (12).

Using Eqs. (9a) and (9b), the variance of the area-average rainfall can be written as

$$\text{var}(R) = \text{cov}(R,r)\frac{f_1}{f_3} = \text{cov}(r,R)\frac{\frac{1}{A^2}\int\int_A \tilde{\rho}(x,y)\,dx^2\,dy^2}{\frac{1}{A}\int_A \tilde{\rho}(x,x_g)\,dx^2} \tag{13}$$

It has to be noticed that Eq. (13) is totally independent of the nugget parameter ρ_0. The variance of the point rainfall is deduced, by expressing the variance of Eq. (5b), as

$$\text{var}(r) = \text{var}(R_g) - \text{var}(B_g) \tag{14}$$

Finally, the nugget parameter can be derived by substituting Eqs. (13) and (14) into Eq. (9b):

$$\rho_0 = \frac{\text{var}(R)}{\frac{\text{var}(r)}{A^2}\int\int_A \tilde{\rho}(x,y)\,dx^2\,dy^2} \tag{15}$$

The normalized representativeness ε_{rep} error can be estimated substituting Eqs. (14) and (15) into Eq. (8). The normalized instrumental radar error $\varepsilon_{\text{rad-inst}}$ can be derived, by expressing the variance of Eq. (5a):

$$\varepsilon^2_{\text{rad-inst}} = \text{var}(A_{\text{rad}}) = \frac{\text{var}(R_{\text{rad}}) - \text{var}(R)}{E(R^2)} \tag{16}$$

The inputs to this approach are the variances of the observed radar rain estimate and gauge rain estimate, as well as the variance of their difference, and finally the point correlation function. The point correlation function $\tilde{\rho}$ (assuming no instant decorrelation) is derived from the 1-h rain radar data (Fig. 4) when a rain threshold of 1 mm/h (or 2 mm/h) is applied, the nugget parameter ρ_0 being estimated through Eq. (15).

As mentioned before all rain measurements are assumed unbiased, which is not the case here (see Table 2). The bias is estimated

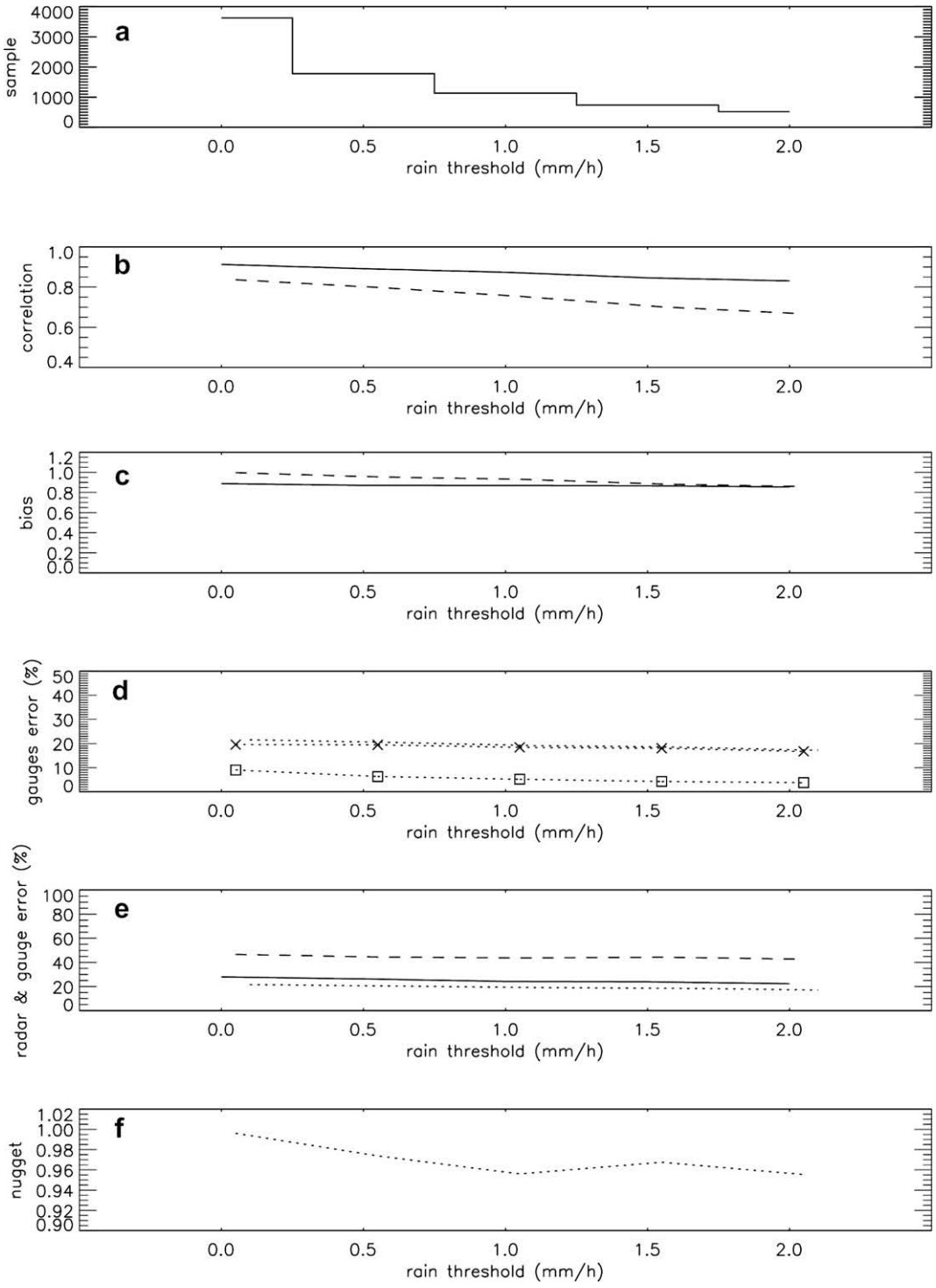

Fig. 6. Error analysis of the one year rain data set. In all the panels, the statistics associated to ZPHI® are in solid line (-), to the classical "*Z*–*R*" algorithm in dashed line (– – –) and to the gauges in dot line (. . .). From the top to the bottom; (a) the sample number used to derive the statistics; (b) the Pearson correlation coefficient; (c) the bias; (d) the instrumental ($\varepsilon_{\text{g-inst}}$) and representativeness (ε_{rep}) gauge error in dot line with square (..□..) and cross (..×..) symbols, respectively. The total gauge error $\left(\sqrt{\varepsilon^2_{\text{g-inst}} + \varepsilon^2_{\text{rep}}}\right)$ is represented by the simple dot line; (e) the radar errors (ε_{rad}) for the two radar algorithms and the gauge error $\left(\sqrt{\varepsilon^2_{\text{g-inst}} + \varepsilon^2_{\text{rep}}}\right)$; (f) the nugget parameter of the point correlation function. On the *x*-axis the rain threshold (in mm/h) applied on the data set.

from the data set, from the slope of the orthogonal regression and removed from the radar rain measurements. The rain gauge data are assumed not biased.

Figs. 6 and 7 show the results of the error analysis applied to the one year data set for 1-h integration time and for all three radar algorithms previously mentioned. On each figure are displayed: the sample number (a), the Pearson correlation of radar versus gauge rain (b), the bias (c), the instrumental and representativeness gauge errors (d), the radar error (e) and the nugget parameter (f).

The robustness of the error analysis to the hypothesis of independent errors is tested by applying different rain thresholds (from 0 mm/h to 2.0 mm/h) to the dataset. Larger rain thresholds reduce considerably the sample number leading to an unstable analysis.

The classical "Z–R" algorithm exhibits a large negative bias increasing with the rain threshold (Fig. 6c). When the radar reflectivity is corrected from the attenuation, the rain estimates shows no bias (Fig. 7c). Using the ZPHI® algorithm causes the bias to be slightly negative (~0.9) and remains constant when considering the various rain thresholds.

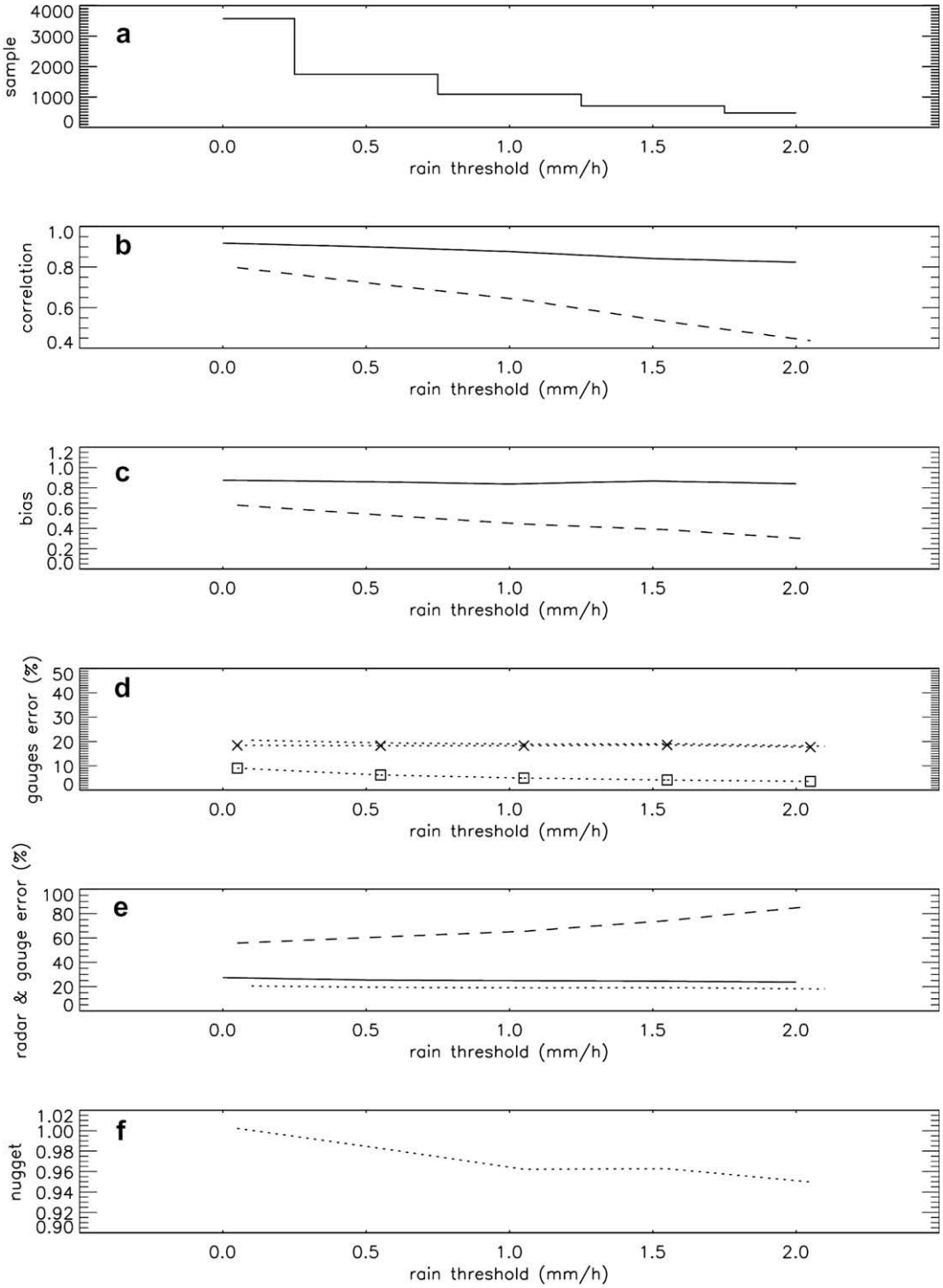

Fig. 7. same as Fig. 6, but for the attenuation corrected "Z_c–R" algorithm instead of classical "Z–R", in dashed line (– – –). ZPHI® algorithm is also shown (·).

The instrumental and representativeness gauge errors are presented in Fig. 6d. The gauge instrumental error decreases from 9% to 4% when the rain threshold increases. The representativeness error (ε_{rep}) is close to 20% when associated to a nugget parameter ranging from 1 to 0.94.

A large radar error (60%) is found with the classical "Z–R" algorithm. With the attenuation correction the radar error is reduced, up to an error of 40%. The ZPHI® algorithm, which includes the attenuation correction, finally leads to an error of 25%, which approaches that of the gauge (Fig. 6e).

Habib and Krajewski [7] quantified the contribution of gauge representativeness error associated with an area of 2 km by 2 km square and 15 min rain accumulation. The contribution of the variance of the gauge error to the variance of radar gauge differences is found to be around (30–45%) for light rain and (40–75%) for heavy rain. In our study, $\mathrm{var}(r - R)/\mathrm{var}(R_g - R_{rad})$ is in the order of (30–40%) when considering R_{rad} the rain estimated by ZPHI®. However, the integration time and area difference make it difficult for the results to be fully comparable.

6. Summary

One of the objectives of the experiment was to validate the rainfall measured by the "Hydrix+ZPHI" radar system, compared with that measured by a network of 25 rain gauges. The results presented in this paper show a reasonably good agreement between the ZPHI®-derived radar rainfall and the gauge measurements. The benefits of ZPHI® in correcting rain "attenuation" and in adjusting the retrieval from DSD "variability" were analyzed and quantified.

The rain variability derived from the radar was compared to that measured by the gauge network, by computing the spatial correlation function. When using the standard Z–R relationship, the spatial correlation drops more rapidly, than that derived from the gauge network. Gebremicheal and Krajewski [6] interpreted similar observations as significant that the radar provides a deteriorated information with respect to the rain gauge network. The correlation function obtained with the polarimetric algorithm ZPHI® improves significantly this picture: the radar derived correlation function really is really close to that from the gauges. However, it should be noticed that the scanning strategy of the radar and the location of the rain gauge network were particularly favorable in the Boigneville experiment.

From the radar alone, thanks to the large number of available samples, an accurate correlation function may be derived from a single rain event. Thus, the influence of time accumulation or type of events (stratiform-convective) can be studied. The correlation radius of intense rain events was found in some instance as small as 2 km, for 6 min integration time.

When comparing radar and gauge rain data, for validation purpose, the various error sources (instrumental and representativeness) should be considered. A new approach has been proposed, to estimate this errors, which allows coexistence of a multiplicative error for the radar, an absolute error for the rain gauge, and a representativeness error (between point measurement and 1 km^2 pixel average) derived from the correlation function.

It was found, based on a 1 year rainfall data base, that the representativeness error is about 20%, while the gauge instrumental error ranges from 9% to 5%. The radar error depends on the algorithm used to derive the rain, with an error of 25% with ZPHI®, an error of 45% with a classical Z_c–R relationship (with Z_c corrected for attenuation) and an error of 60% with a classical Z–R relationship (with observed Z attenuated). Such an approach will be extended to other rain datasets characteristic of mountainous Mediterranean events, in the context of the FRAMEA (Flood forecasting using Radar in Alpine and Mediterranean Area) project.

Acknowledgements

The authors would like to thanks the French research ministry for his support to the CITRAM project and ARVALIS-Institut-du-Végétal for providing rain gages data.

References

[1] Le Bouar E, Testud J. Validation of the rain profiling algorithm ZPHI from the C-band polarimetric weather radar in Darwin. J Atmos Ocean Technol 2001;18:1819–37.
[2] Ciach GJ, Krajewski WF. On the estimation of radar rainfall error variance. Adv Water Resour 1999;22(6):585–95.
[3] Ciach GJ. Local random errors in Tipping–Bucket rain gauge measurements. J Atmos Ocean Technol 2003;20:752–9.
[4] Cressman GW. An operational objective analysis system. Mon Weather Rev 1959;87:367–74.
[5] Doviak RJ, Zrnic DS. Doppler radar and weather observations. Academic Press; 1984. p. 97, 458 pp.
[6] Gebremichael M, Krajewski WF. Assessment of the statistical characterization of small-scale rainfall variability from radar: analysis of TRMM ground validation datasets. J Appl Meteorol 2004;43:1180–99.
[7] Habib E, Krajewski WF. Uncertainty analysis of the TRMM ground-validation radar–rainfall products: application to the TEFLUN-B field campaign. J Appl Meteorol 2002;41:558–72.
[8] Habib E, Ciach GJ, Krajewski WF. A method for filtering out rain gage representativeness errors from the verification distribution of radar and rain gauge rainfall. Adv Water Resour 2004;27:967–80.
[9] Krajewski WF, Ciach GJ, Habib E. An analysis of small-scale rainfall variability in different climatic regimes. Hydrol Sci 2003;48(2):151–62.
[10] Meehl GA, Stocker TF, Collins WD, Friedlingstein P, Gaye AT, Gregory JM, et al. Global climate projections. In: Qin SD, Manning M, Chen Z, Marquis M, Averyt KB, et al., editors. Climate change 2007: the physical science basis. Contribution of working group I to the fourth assessment report of the intergovernmental panel on climate change solomon. Cambridge, United Kingdom and New York, NY, USA: Cambridge University Press; 2007.
[11] Nash JE, Sutcliffe JV. River flow forecasting through conceptual models Part I — a discussion of principles. J Hydrol 1970;10(3):282–90.
[12] Paulson KS. Fractal interpolation of rain rate time series. J Geophys Res 2004;109:D22102.
[13] Shimizu K. A bivariate log normal distribution with an analysis of rainfall data. J Appl Meteor 1993;32:161–71.
[14] Testud J, Le Bouar E, Obligis E, Ali-Meheni M. The rain profiling algorithm applied to polarimetric weather radar. J Atmos Ocean Technol 2000;17:332–56.
[15] Testud J, Oury S, Black RA, Amayenc P, Dou X. The concept of normalized" distribution to describe raindrop spectra: a tool for cloud physics and cloud remote sensing. J Appl Meteorol 2001;40:1118–40.
[16] Zhang Y, Adams T, Bonta JV. Subpixel-scale rainfall variability and the effects on separation of radar and gauge rainfall errors. J Hydrometeorol 2007;8:1348–63.